

Majorana constellations for optical scalar beams and vector fields

F. Torres-Leal,^{1,*} E. García Herrera,^{1,*} M. P. Morales Rodríguez,^{2,*} B. Perez-Garcia,^{1,†} and B. M. Rodríguez-Lara^{3,‡}

¹*Photonics and Mathematical Optics Group,
Tecnologico de Monterrey, Monterrey 64849, Mexico*

²*Departamento de Física Teórica, Atómica y Óptica,
Universidad de Valladolid, 47011 Valladolid, Spain*

³*Universidad Politécnica de Pachuca. Carr. Pachuca-Cd. Sahagún Km.20,
Ex-Hda. Santa Bárbara. Zempoala, 43830 Hidalgo, Mexico*

(Dated: December 30, 2024)

Abstract

We explore the Majorana stellar representation on the Riemann sphere for optical scalar beams and vector fields, utilizing the spin and orbital angular momentum of light. In this framework, star constellations for scalar Laguerre-Gaussian beam basis appear at the poles of the sphere, while those for vector fields correspond to well-defined circular polarizations. Leveraging the $su(2)$ symmetry of angular momentum, we populate the sphere through generalized unitary rotations of basis elements, producing optical analogues of Bloch and generalized $su(2)$ coherent states for both scalar beams and vector fields. These rotations position constellations for scalar Hermite-Gaussian beams and vector Hermite-Gaussian partial Poincaré fields, restricted to linear polarization, along the equator of the sphere. We also address the inverse problem, reconstructing optical scalar beams and vector fields from their stellar constellations. Additionally, we explore scalar and vector analogues of cat codes and kings of quantumness, contributing to the visualization and characterization of complex optical beams and fields. These insights suggest potential applications in optical communications.

* These authors contributed equally to this work.

† e-mail: b.pegar@tec.mx

‡ e-mail: bmlara@upp.edu.mx; blas.rodriguez@gmail.com

I. INTRODUCTION

Light propagating through homogeneous, isotropic, and linear media models as a transverse electromagnetic field. The electric and magnetic field vectors are perpendicular to each other and to the direction of propagation. The temporal behavior of the electric field determines its polarization, characterized by the path traced by the electric field vector over time. The most general path is an ellipse in the plane transverse to propagation, known as elliptical polarization. This polarization can rotate in either a clockwise or counter-clockwise direction as viewed from the direction of propagation, with special cases including circular and linear polarization [1, 2].

Using Jones calculus, horizontal and vertical linear polarization vectors correspond to eigenstates of the Pauli-Z matrix. The diagonal and anti-diagonal linear polarization vectors correspond with those of the Pauli-X matrix, while the left and right circular polarization vectors align with the eigenstates of the Pauli-Y matrix [3, 4]. Thus, polarization shows an underlying symmetry provided by the special unitary $su(2)$ Lie algebra with Bargmann parameter $j = 1/2$, which matches intrinsic angular momentum [5]. In this representation, the four Stokes parameters,

$$S_j = \langle \hat{\sigma}_j \rangle, \quad (1)$$

are the mean expected value of the identity $\hat{\sigma}_0$ and three Pauli matrices $\hat{\sigma}_j$ with $j = x, y, z$, and map into the Poincaré sphere. Each totally polarized state corresponds to a point on the surface of the sphere, whereas those inside correspond to partially polarized states.

The spatial degree of freedom provides another angular momentum component that may be intrinsic or extrinsic [6]. A standard choice to construct a basis for intrinsic orbital angular momentum (OAM) are Laguerre-Gaussian beams (LGBs) [7],

$$\Phi_{p,\ell}(r, \phi, z) = \frac{w_0}{w(z)} e^{\frac{-ikr^2}{2R(z)}} e^{i(2p+|\ell|+1)\varphi(z)} e^{-\frac{r^2}{w^2(z)}} \left(\frac{\sqrt{2}r}{w(z)} \right)^{|\ell|} L_p^{|\ell|} \left(\frac{2r^2}{w^2(z)} \right) e^{i\ell\phi}, \quad (2)$$

for their well-defined hyperbolic [8] and angular [9] momenta proportional to the radial number p and the azimuthal number ℓ , respectively. We use the standard definitions for the beam waist $w(z) = w_0 \sqrt{1 + (z/z_R)^2}$, curvature radius $R(z) = z [1 + (z_R/z)^2]$, and Gouy phase $\varphi(z) = \arctan(z/z_R)$, in terms of the propagation distance z , the propagation number $k = 2\pi/\lambda$, the initial waist $w_0 = \lambda/(\pi\theta)$, and the Rayleigh range $z_R = kw_0^2/2$, in terms of the wavelength λ and beam divergence θ in the media.

Just as the spin representation of the $su(2)$ Lie algebra describes light polarization, the OAM representation with Dicke states $|j; m\rangle$, with Bargmann parameter $j = (2p + |\ell|)/2 = 0, 1/2, 1, 3/2, \dots$ and its projection along the propagation axis $m = \ell/2 = -j, -j+1, \dots, j-1, j$, helps our understanding of the orbital angular momentum of light [10]. For instance, using Clebsch-Gordan coefficients to calculate the total angular momentum and characterize vector fields that have both polarization and orbital angular momentum. However, visualization of these states presents its own challenges. The subspace with Bargmann number $j = 0$ is a single point representing the standard Gaussian beam $\psi_{0,0}$. The LGBs $\psi_{0,1}$ and $\psi_{0,-1}$, which map into the south and north poles of the Bloch-Poincaré sphere, span the subspace with $j = 1/2$. Subspaces for higher-dimensional orbital angular momenta with Bargmann parameter j require $2j + 1$ LGBs as an orthogonal basis, which maps onto a $(2j + 1)$ -dimensional Bloch hyper-sphere.

Majorana stellar representation provides a geometric representation for states within systems possessing a symmetry with an underlying $su(2)$ Lie algebra [11–13]. This approach maps a pure state, built through the coherent superposition of OAM Dicke states, into a complex polynomial. Projecting the complex roots of this polynomial stereographically onto the Riemann sphere offers a visual representation of the state. Thus, a state in a subspace with Bargmann parameter j appears as a constellation of up to $2j$ Majorana stars. The Majorana representation has proven invaluable for various applications in quantum physics and quantum optics. It has been used to characterize the quantum polarization of light [14, 15], map structured-Gaussian beams into a modal Majorana constellation [16], study the geometrical phases of coherent states of higher-spin [17], represent anticoherent spin states [18], multipolar highly-quantum states [19], and in rotation sensing using king of quantumness states [20–22]. Thus, the Majorana representation is an alternative way to describe quantum states, especially in spin systems.

Visualization techniques for structured light with angular momentum have advanced significantly [23], beginning with the Modal Poincaré Sphere, which was developed to represent first-order scalar beams with orbital angular momentum [24] and later expanded to third-order modes [25]. This approach was instrumental in visualizing astigmatic transformations by effectively mapping them onto the sphere [26]. The Higher-order Poincaré Sphere (HOPS) was introduced to address polarization states, offering an extended framework to represent beams with both spin and orbital angular momenta, such as radially and azimuthally polar-

ized cylindrical vector beams, as they propagate through anisotropic or nonlinear media [27]. The Hybrid-order Poincaré Sphere (HyOPS) further generalized this concept to accommodate cases where spin and orbital angular momenta interact dynamically in inhomogeneous anisotropic media, allowing for conversion between them [28]. Recently, the $SU(2)$ Poincaré Sphere was introduced to generalize these models, capturing a broader family of structured light with multidimensional ray-wave structures. This approach reveals a unified view where previous Poincaré sphere models are special cases, and it supports higher-dimensional state tailoring for applications across optics and quantum information [29]. In contrast, the Majorana stellar representation offers a flexible alternative, allowing any structured Gaussian beam to be visualized as a constellation on the Riemann sphere [16].

Here, we revisit Majorana stellar representation to describe optical scalar beams, extend it for vector fields by incorporating total angular momentum, and introduce the inverse problem of reconstructing optical scalar beams and vector fields from their constellations. First, we show how to construct Majorana constellations for scalar light beams, using LGBs as the building basis, in Section II. Then, we populate the Riemann sphere using the optical analogy of Bloch and Generalized Coherent States for the $su(2)$ Lie algebra [30, 31], exploring optical analogies for cat codes. In addition, we introduce the inverse problem of reconstructing optical scalar beams from a Majorana constellation given by the vertices of platonic solids leading to the optical analogues of the so-called king of quantumness states. Using Clebsch-Gordan coefficients to add the polarization and orbital angular momentum of light into total angular momentum, we build the constellations of full vector fields in Section III. For the sake of completeness, we explore the vector field analogies of the scalar beams discussed in Section II. We close with our conclusions in Section IV.

II. MAJORANA CONSTELLATIONS FOR SCALAR LIGHT BEAMS

Let us begin by discussing the construction of Majorana constellations in the scalar Laguerre-Gaussian beam (LGB) basis. We define the orthonormal scalar LGB,

$$\Phi_{p,\ell}(r, \phi, z) = \frac{\sqrt{2}}{w(z)} e^{-i\frac{kr^2}{2R(z)}} e^{i(2p+|\ell|+1)\varphi(z)} \psi_{n_+,n_-} \left(\frac{\sqrt{2}r}{w(z)}, \phi \right), \quad (3)$$

in terms of the Laguerre-Gaussian modes (LGMs) [31, 32],

$$\psi_{n_+,n_-}(q_\rho, q_\phi) = (-1)^p \sqrt{\frac{p!}{\pi(p+|\ell|)!}} q_\rho^{|\ell|} e^{-\frac{1}{2}q_\rho^2} L_p^{|\ell|}(q_\rho^2) e^{i\ell q_\phi}, \quad (4)$$

which are eigenmodes of the isotropic two-dimensional quantum oscillator with the left- and right-handed numbers $n_\pm = 0, 1, 2, \dots$. We use the shorthand notation $q_\rho = \sqrt{2}r/w(z)$ and $q_\phi = \phi$ for the sake of space. The radial and azimuthal numbers reduce to the following expressions,

$$\begin{aligned} p &= \frac{1}{2}(n_+ + n_- - |n_+ - n_-|), \\ \ell &= n_+ - n_-. \end{aligned} \quad (5)$$

The LGMs provide a complete, orthonormal basis,

$$\int_0^\infty dq_\rho \int_0^{2\pi} dq_\phi q_\rho \psi_{m_+,m_-}^*(q_\rho, q_\phi) \psi_{n_+,n_-}(q_\rho, q_\phi) = \delta_{m_+,n_+} \delta_{m_-,n_-}, \quad (6)$$

for the Hilbert space of square-integrable functions on the dimensionless real plane (q_ρ, q_ϕ) in polar coordinates. At $z = 0$, we recover LGMs from LGBs. Our analysis focuses on the former, although it remains valid for the latter as well.

It is straightforward to connect LGMs with the OAM Dicke basis [30, 31],

$$\langle q_\rho, q_\phi | j; m \rangle = \psi_{j+m, j-m}(q_\rho, q_\phi), \quad (7)$$

with the parameter $m = -j, -j+1, \dots, j-1, j$. Thus, each subspace comprises $2j+1$ LGMs that conserve the Bargmann parameter $j = (n_+ + n_-)/2 = (2p + |\ell|)/2$. Majorana's stellar representation for visualization of higher-dimensional angular momentum states associates a polynomial [11],

$$p_\psi(\zeta) = \sum_{m=-j}^j (-1)^{j-m} \sqrt{\binom{2j}{j-m}} c_m \zeta^{j+m}, \quad (8)$$

to any state in these Hilbert subspaces,

$$\psi(q_\rho, q_\phi) = \sum_{m=-j}^j c_m \psi_{j+m, j-m}(q_\rho, q_\phi), \quad (9)$$

with $c_m \in \mathbb{C}$ such that $\sum_{m=-j}^j |c_m|^2 = 1$. The Majorana polynomial has $2j$ complex roots ζ_j as long as $c_m \neq 0$. If one or more coefficients c_m are zero, then $\zeta_j = \infty$ is a root of

multiplicity equal to the number of zeros. Each complex root ζ_j can be stereographically projected onto the Riemann sphere,

$$(x_j, y_j, z_j) = \left(\frac{2\text{Re}(\zeta_j)}{1 + |\zeta_j|^2}, \frac{2\text{Im}(\zeta_j)}{1 + |\zeta_j|^2}, \frac{1 - |\zeta_j|^2}{1 + |\zeta_j|^2} \right), \quad (10)$$

with roots of zero value mapping onto the north pole and those with infinite value onto the south pole.

We slightly deviate from Majorana's method. Usually, any given state in the Dicke basis $|j; m\rangle$, corresponding to the LGM with $n_+ = j + m$ and $n_- = j - m$, maps onto $j - m$ stars at the north pole with no stars at the south pole, except for $m = j$ which maps into $2j$ stars at the south pole with no stars at the north pole. Instead, we introduce $j + m$ stars in the south pole to create constellations composed of $2j$ Majorana stars. The state $|j; m\rangle$ is represented by $j - m$ stars at the north pole with $j + m$ stars at the south pole. This arrangement allows us to use the number of stars at the poles to determine the left- and right-handed numbers of the LGM, facilitating the recovery of the radial and azimuthal numbers. Figure 1 illustrates the Majorana constellations for the Dicke states $|j, m\rangle$ spanning the subspaces with Bargmann parameter $j = 1/2, 1, 3/2$. The size of the point on the Riemann sphere is directly proportional to the number of stars. We also show the intensity and phase distribution for the corresponding LGMs.

A. Bloch and Generalized Coherent States

Now, let us populate the Riemann sphere. The $su(2)$ Lie algebra provides a general unitary rotation [31, 33],

$$\begin{aligned} \hat{R}(\vartheta, \varphi) &= e^{\vartheta(e^{i\varphi}\hat{J}_+ - e^{-i\varphi}\hat{J}_-)}, \\ &= e^{i\varphi\hat{J}_z} e^{i2\vartheta\hat{J}_y} e^{-i\varphi\hat{J}_z}, \\ &= \sum_{p,q=0}^{2j} (-1)^{(j-p)} e^{i\varphi(p-q)} \sin^{2j} \vartheta \tan^{-(p+q)} \vartheta \sqrt{\binom{2j}{j-p} \binom{2j}{j-q}} \times \dots \\ &\quad \dots \times {}_2F_1 [p - j, q - j; -2j; \csc^2 \vartheta] |j; p\rangle \langle j; q|, \end{aligned} \quad (11)$$

which corresponds to a 2ϑ rotation around the y -axis and a φ rotation around the z -axis of the sphere. In this context, ϑ serves as the polar angle, ranging from 0 to $\pi/2$, and φ as the azimuthal angle, ranging from 0 to 2π .

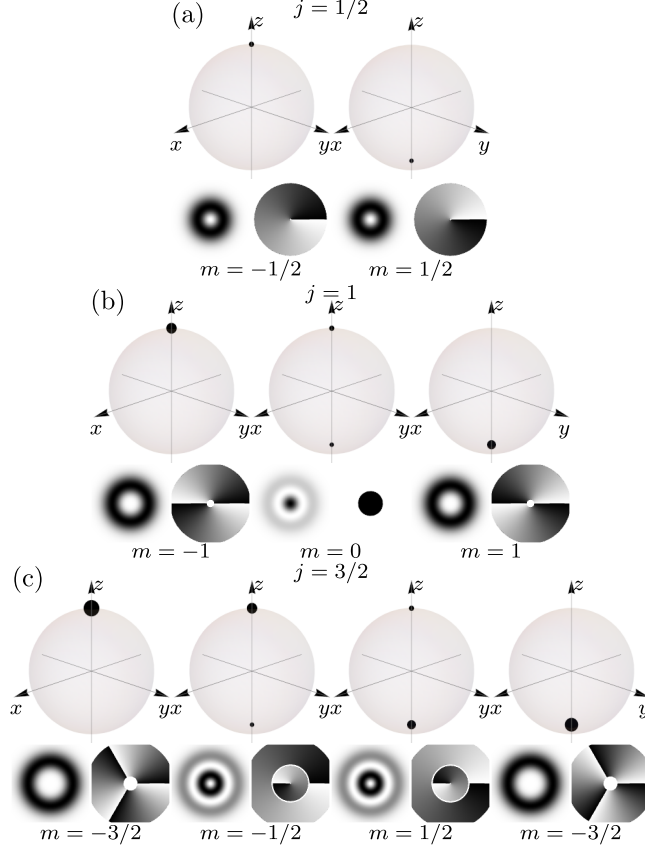


FIG. 1. Majorana constellation for optical scalar light beam analogue of the OAM Dicke states $\langle q_\rho, q_\phi | j; m \rangle = \psi_{j+m, j-m}(q_\rho, q_\phi)$ spanning the subspace with Bargmann parameter (a) $j = 1/2$ with one star, (b) $j = 1$ with two stars, and (c) $j = 3/2$ with three stars per constellation, as well as the intensity and phase distribution for the corresponding LGM. The size of the point on the Riemann sphere is directly proportional to the number of stars.

This rotation acting on the lowest LGMs basis of the corresponding OAM Dicke basis,

$$\psi_{\vartheta, \varphi}(q_\rho, q_\phi) = (e^{i\varphi} \sin \vartheta)^{2j} \sum_{k=0}^{2j} \sqrt{\binom{2j}{k}} (e^{i\varphi} \tan \vartheta)^{-k} \psi_{2j-k, k}(q_\rho, q_\phi), \quad (12)$$

yields the optical analogy of Bloch coherent states [30]. They form an over complete,

$$\int_0^\infty dq_\rho q_\rho \int_0^{2\pi} dq_\phi \psi_{\tilde{\vartheta}, \tilde{\varphi}}^*(q_\rho, q_\phi) \psi_{\vartheta, \varphi}(q_\rho, q_\phi) = \left(\csc \vartheta \csc \tilde{\vartheta} \right)^j \left[e^{\frac{i}{2}(\varphi - \tilde{\varphi})} \sin \vartheta \sin \tilde{\vartheta} + e^{-\frac{i}{2}(\varphi - \tilde{\varphi})} \cos \vartheta \cos \tilde{\vartheta} \right]^{2j}, \quad (13)$$

basis for states for the Hilbert space subspace with Bargmann parameter j . Figure 2 shows

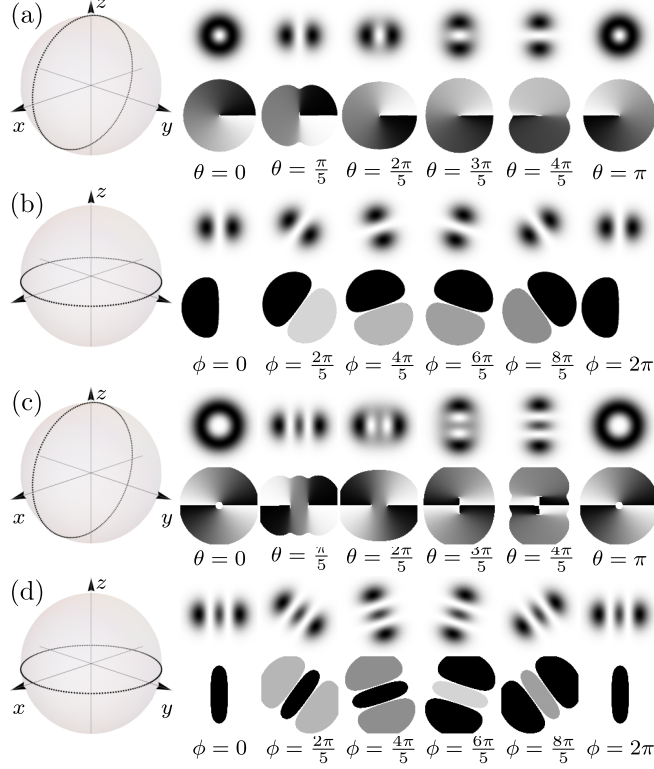


FIG. 2. Majorana constellations, irradiance, and phase distributions for the optical scalar light beam analog of Bloch coherent states (a) and (c) $\psi_{\vartheta,0}(q_\rho, q_\phi)$ and (b) and (d) $\psi_{\pi/4,\varphi}(q_\rho, q_\phi)$ for (a)-(b) $j = 1/2$ and (c)-(d) $j = 1$.

optical analogy of Bloch coherent states $\psi_{\vartheta,0}(q_\rho, q_\phi)$ and $\psi_{\pi/4,\varphi}(q_\rho, q_\phi)$ for Bargmann parameters $j = 1/2, 1$.

Generalized Gilmore-Perelomov coherent states for the $su(2)$ Lie algebra arise from the rotation of any LGMs of the OAM Dicke basis [33],

$$\begin{aligned}
 \psi_{\vartheta,\varphi,m}(q_\rho, q_\phi) = & \sqrt{\binom{2j}{j-m}} \sec^{-2j} \vartheta (e^{i\varphi} \tan \vartheta)^j \times \\
 & \times \sum_{k=0}^{2j} (-1)^k \sqrt{\binom{2j}{k}} e^{-i\varphi(k+m)} \tan^{(k-m)} \vartheta \times \\
 & \times {}_2F_1(-k, -j+m; -2j; \csc^2 \vartheta) \psi_{2j-k,k}(q_\rho, q_\phi),
 \end{aligned} \tag{14}$$

that allow us to populate the Riemann sphere with less clustered constellations. For example, if we rotate the LGM $\psi_{k,2j-k}(q_\rho, q_\phi)$, that has a constellation with k stars in the south pole and $2j - k$ stars in the north pole, we obtain a constellation with all its stars rotated by a

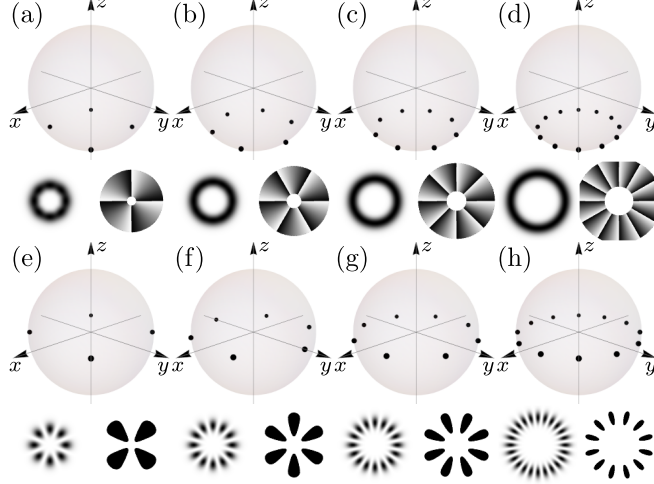


FIG. 3. Majorana constellations, irradiance, and phase distributions for scalar light beams analogues of the zeroth cat code with (a)-(d) $\vartheta = \pi/8$ and (e)-(h) $\vartheta = \pi/4$, and $\varphi = 0$ for (a),(e) $j = 2$, (b),(f) $j = 3$, (c),(g) $j = 4$, and (d),(h) $j = 6$.

ϑ angle around the z -axis and φ angle around the y -axis.

It is straightforward to realize that the Hermite-Gauss modes (HGMs) are generalized coherent states of the LGMs [34],

$$\begin{aligned}
 \psi_{n_x, n_y}^{(HG)}(q_x, q_y) &= (-i)^{n_x} \psi_{\pi/4, 0, (n_x - n_y/2)}(q_\rho, q_\phi), \\
 &= (-i)^{n_x} 2^{-\frac{1}{2}(n_x + n_y)} \sqrt{\binom{n_x + n_y}{n_y}} \times \\
 &\quad \times \sum_{k=0}^{2j} (-1)^k \sqrt{\binom{n_x + n_y}{k}} {}_2F_1[-n_y, -k; -n_x - n_y; 2] \psi_{n_x + n_y - k, k}(q_\rho, q_\phi),
 \end{aligned} \tag{15}$$

in the Bargmann subspace $j = (n_x + n_y)/2$ with horizontal $n_x = j - m$ and vertical $n_y = j + m$ numbers. Thus, the HGMs Majorana constellation will consist of n_x stars at the point $(x, y, z) = (1, 0, 0)$ and n_y stars at the point $(-1, 0, 0)$ on the Riemann sphere. The equator of the Riemann sphere will contain rotated HGMs with inclination angle equal to the azimuthal angle φ , Fig. 2(b) and Fig. 2(d).

B. Cat codes and Kings of Quantumness

In quantum information theory, cat codes refer to quantum error correction codes that utilize superposition of coherent states [35–38],

$$|C_\alpha^n\rangle = \frac{1}{2d\sqrt{\mathcal{N}_\alpha^n}} \sum_{k=0}^{2d-1} e^{-\frac{i\pi}{d}kn} |e^{\frac{i\pi}{d}k}\alpha\rangle, \quad (16)$$

where α is the coherent parameter, \mathcal{N} is a normalization constant, the size of the basis is $2d$ with $d \geq 2$, and $n = 0, 1, 2, \dots, 2d - 1$. They are an extension to Schrödinger cat states, designed to be robust against phase errors. It is straightforward to recognize that the optical analogy of these codes in the Hilbert subspaces with constant Bargmann parameter j ,

$$|C_{\vartheta,\varphi}^m\rangle = \frac{1}{\sqrt{\mathcal{N}_{\vartheta,\varphi}^m}} \sum_{k=0}^{2j-1} e^{-\frac{i\pi}{j}km} \hat{R}(\vartheta, \varphi + \pi k/j) |j; -j\rangle, \quad (17)$$

with sum modulus 2π for the phase, normalization constant $\mathcal{N}_{\vartheta,\varphi}^m$, and cat code index $m = 1, 2, \dots, 2j - 1$, yield the LGMs spanning the subspace,

$$\langle q_\rho, q_\phi | C_{\vartheta,\varphi}^0 \rangle = \frac{1}{\sqrt{\cos^{4j}\vartheta + \sin^{4j}\vartheta}} \left[\cos^{2j}\vartheta \psi_{2j,0}(q_\rho, q_\phi) + (e^{i\varphi} \sin\vartheta)^{2j} \psi_{0,2j}(q_\rho, q_\phi) \right], \quad (18)$$

$$\langle q_\rho, q_\phi | C_{\vartheta,\varphi}^m \rangle = e^{im\varphi} \psi_{2j-m,m}(q_\rho, q_\phi),$$

with the exception of the zeroth cat code, which provides a superposition of the first and last OAM Dicke states in the basis. The Majorana constellation for the zeroth cat code appears on the $2(\pi/2 - \vartheta)$ parallel of the Riemann sphere, with its stars distributed equidistantly and rotated by an azimuthal angle φ , Fig. 3.

It is also possible to produce a scalar light beam from a given Majorana constellation, effectively solving an inverse problem. First, we recover the roots ζ_j of the Majorana polynomial from the Majorana constellation by applying the stereographic projection,

$$\zeta_j = \frac{x_j + iy_j}{1 + z_j}, \quad (19)$$

that maps points (x_j, y_j, z_j) on the Riemann sphere to the complex plane, where the north pole $(0, 0, 1)$ maps to the origin and the south pole $(0, 0, -1)$ to a point at infinity. These complex values serve as the roots of the Majorana polynomial,

$$\begin{aligned} p_\psi(\zeta) &= d_j \prod_{m=-j}^j (\zeta - \zeta_m), \\ &= \sum_{m=-j}^j d_m \zeta^{j+m}, \end{aligned} \quad (20)$$

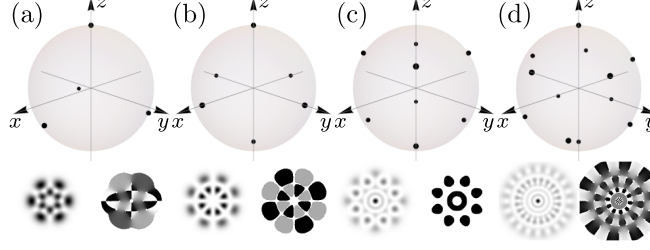


FIG. 4. Majorana constellations, irradiance, and phase distributions for scalar light beams which stars locate at the vertices of four platonic solids: (a) tetrahedron $j = 2$, (b) octahedron $j = 3$, (c) hexahedron $j = 4$, and (d) dodecahedron $j = 6$.

associated with the scalar light beam ψ , where we define the shorthand notation $d_m = (-1)^{j-m} \sqrt{\binom{2j}{j-m}} c_m$. Using, Vieta's formulas [39],

$$\frac{d_m}{d_j} = (-1)^{j-m} \sum_{-j \leq p-j \leq p-j+1 \leq \dots \leq j} \prod_{q=-j}^j \zeta_{p_q+j+1}, \quad (21)$$

we can determine the modified coefficients d_m for $m = -j, -j+1, \dots, j-1$, while we recover the final coefficient d_j from the normalization condition $\sum_{m=-j}^j |d_m|^2 = 1$. From the modified coefficients d_m , it is straightforward to recover recover the coefficients c_m ,

$$c_m = (-1)^m \sqrt{\frac{j!(j+m)!}{(2j)!}} d_m, \quad (22)$$

for the superposition of the corresponding LGMs in the Bargmann subspace. For example, starting from a Majorana constellation given by the vertices coordinates of a Platonic solid in the Riemann sphere [40], we can generate their corresponding scalar light beam, Fig. 4. These states are the optical analogues of the kings of quantumness used for sensing rotations while establishing the coordinate system for quantum communications [20, 21].

III. MAJORANA CONSTELLATIONS FOR VECTOR FIELDS

It is a standard occurrence in polarimetry to map polarization onto the Poincaré sphere. This is equivalent to assigning polarization an intrinsic angular momentum representation with Bargmann parameter $j = 1/2$, such that the states $|1/2, \pm 1/2\rangle \equiv \epsilon_{\pm 1/2}$ represent left- and right-handed circular polarization. Integrating the polarization and spatial degrees of

freedom leads to light fields,

$$\boldsymbol{\psi}(q_\rho, q_\phi) = \sum_{j=0}^{\infty} \sum_{m=-j}^j \sum_{k=-1/2}^{1/2} c_{j,m,k} \psi_{j+m, j-m}(q_\rho, q_\phi) \boldsymbol{\epsilon}_k, \quad (23)$$

constructed, for example, by the superposition of spatially dependent scalar Laguerre-Gaussian beams and spatially independent polarization vectors. The analogy of polarization and spatial degrees of freedom with spin and angular momenta allows us to rewrite these light fields,

$$\boldsymbol{\psi}(q_\rho, q_\phi) = \sum_{J=0}^{\infty} \sum_{M=-J}^J C_{J;M} \boldsymbol{\Psi}_{J;M}(q_\rho, q_\phi), \quad (24)$$

in the total angular momentum (TAM) Dicke basis,

$$\boldsymbol{\Psi}_{J;M}(q_\rho, q_\phi) = \sum_{m_s=-j_s}^{j_s} \sum_{m_p=-1/2}^{1/2} c_{j_s, m_s, j_p, m_p}^{J, M} \psi_{j_s+m_s, j_s-m_s}(q_\rho, q_\phi) \boldsymbol{\epsilon}_{m_p}, \quad (25)$$

where the Clebsch-Gordan coefficients $c_{j_s, m_s, j_p, m_p}^{J, M}$ provide the precise weights for each possible combination of spin and orbital angular momenta required to construct a well-defined total angular momentum state [41, 42].

A TAM Bargmann parameter J decomposes into polarization and spatial parameters $j_p = 1/2$ and $j_s = |J - 1/2|$, respectively. Thus, TAM $J = 0$ corresponds to the singlet $[\psi_{1,0}(q_\rho, q_\phi) \boldsymbol{\epsilon}_{-1/2} - \psi_{0,1}(q_\rho, q_\phi) \boldsymbol{\epsilon}_{1/2}]/2$ providing linear polarization for $M = 0$. TAM $J = 1/2$ corresponds to a spatial $j_s = 0$; that is, the Gaussian beam $\psi_{0,0}(q_\rho, q_\phi) \boldsymbol{\epsilon}_{\pm 1/2}$ providing right- and left-handed circular polarization for $M = -1/2$ and $M = 1/2$, respectively, Fig. 5(a). TAM $J = 1$ corresponds to a spatial $j_s = 1/2$ with $m_s = -1/2$, yielding $\psi_{0,1}(q_\rho, q_\phi) \boldsymbol{\epsilon}_{-1/2}$, providing right-handed circular polarization for $M = -1$, the superposition of $m_s = \pm 1/2$ with right- and left-handed circular polarization $[\psi_{1,0}(q_\rho, q_\phi) \boldsymbol{\epsilon}_{-1/2} + \psi_{0,1}(q_\rho, q_\phi) \boldsymbol{\epsilon}_{1/2}]/2$, providing linear polarization for $M = 0$, and $m_s = 1/2$, yielding $\psi_{1,0}(q_\rho, q_\phi) \boldsymbol{\epsilon}_{-1/2} \boldsymbol{\epsilon}_{1/2}$, providing left-handed circular polarization for $M = 1$, Fig. 5(b). The extremes of the TAM ladder, $M = \pm J$, show well-defined right- and left-handed circular polarization, while the intermediate states show a coherent superposition of them, Fig. 5(c). For visualization and clarity purposes, Fig. 6 presents the polarization distribution for the vector light fields $\boldsymbol{\Psi}_{J;M}(q_\rho, q_\phi)$ analogues to TAM Dicke states with parameters $\{J, M\}$, with scaling adjusted for illustrative purposes.

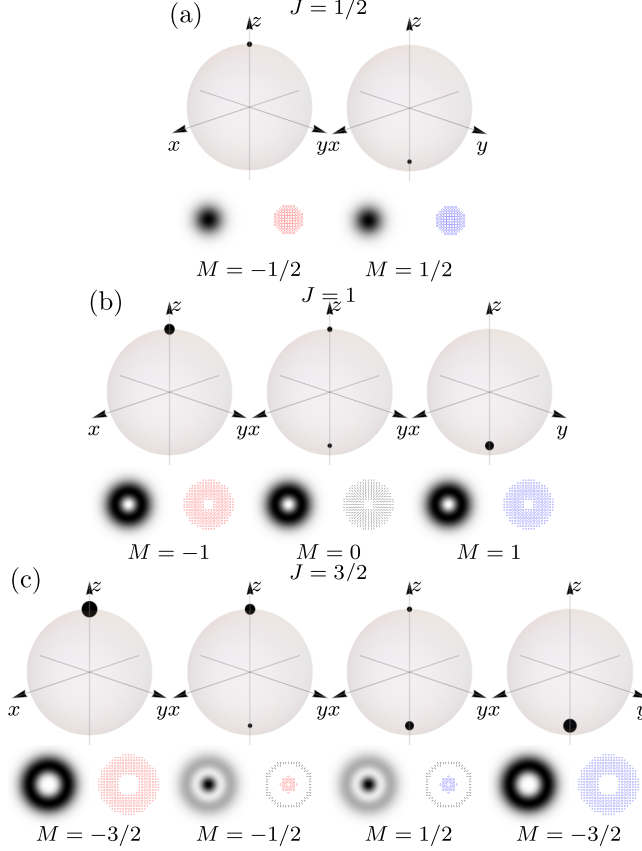


FIG. 5. (Color online) Majorana constellations for vector light fields $\Psi_{J,M}(q_\rho, q_\phi)$ analogues to TAM Dicke states, spanning subspace with Bargmann parameters (a) $J = 1/2$ with one star, (b) $J = 1$ with two stars, and (c) $J = 3/2$ with three stars per constellation. Each set shows the Majorana constellation (top), alongside the intensity (bottom left) and polarization distribution (bottom right) of the vector light field. Red, blue and black indicates left-handed, right-handed, and linear polarization, respectively.

A. Bloch and Generalized Coherent States

To populate the Riemann sphere for vector fields, we use the general unitary rotation for the $su(2)$ algebra $\hat{R}(\vartheta, \varphi)$ acting on the lowest vector field mode $\Psi_{J,-J}(q_\rho, q_\phi)$ to obtain,

$$\Psi_{\vartheta, \varphi}(q_\rho, q_\phi) = (e^{i\varphi} \sin \vartheta)^{2J} \sum_{k=0}^{2J} \sqrt{\binom{2J}{k}} (e^{i\varphi} \tan \vartheta)^{-k} \Psi_{2J-k;k}(q_\rho, q_\phi), \quad (26)$$

vector light fields analogues of Bloch coherent states. Figure 7 shows vector fields $\Psi_{\vartheta,0}(q_\rho, q_\phi)$ and $\Psi_{\pi/4,\varphi}(q_\rho, q_\phi)$ for TAM Bargmann parameters $J = 1, 3/2$. Only the poles possess a

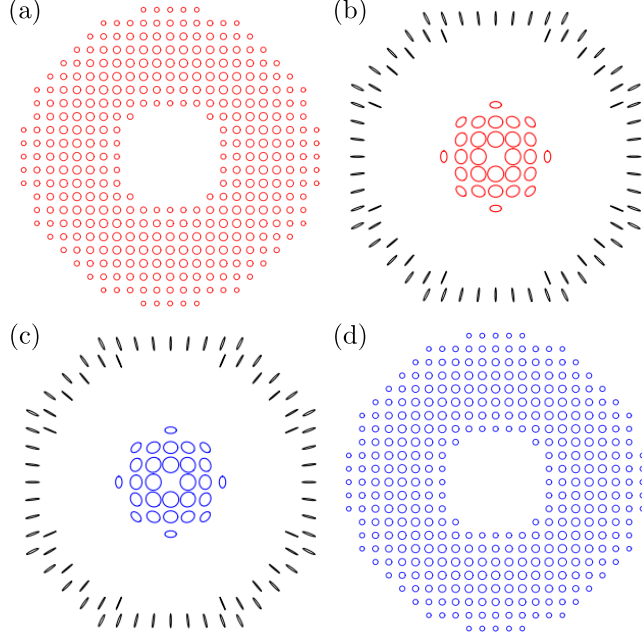


FIG. 6. (Color online) Polarization distribution for the vector light fields $\Psi_{J,M}(q_\rho, q_\phi)$ analogues to TAM Dicke states with parameters $\{J, M\}$ equal to (a) $\{3/2, -3/2\}$, (b) $\{3/2, -1/2\}$, (c) $\{3/2, 1/2\}$, and (d) $\{3/2, -3/2\}$. Red, blue and black indicates left-handed, right-handed, and linear polarization, respectively.

well defined polarization a generalized coherent state shows a position dependent polarization. The equator correspond to partial Poincaré fields restricted to linear polarization with Hermite-Gaussian spatial profile [43], Fig. 7(b) and Fig. 7(d).

Generalized Gilmore-Perelomov coherent states for the $su(2)$ Lie algebra arise from the rotation of any vector field of the TAM Dicke basis [44, 45],

$$\begin{aligned}
 \Psi_{\vartheta, \varphi, M}(q_\rho, q_\phi) &= \sqrt{\binom{2J}{J-M}} \sec^{-2J} \vartheta (e^{i\varphi} \tan \vartheta)^J \times \\
 &\times \sum_{k=0}^{2J} (-1)^k \sqrt{\binom{2j}{k}} e^{-i\varphi(k+M)} \tan^{(k-M)} \vartheta \times \\
 &\times {}_2F_1(-k, -J+M; -2j; \csc^2 \vartheta) \Psi_{2J-k; k}(q_\rho, q_\phi),
 \end{aligned} \tag{27}$$

which allow us to populate the Riemann sphere with less clustered constellations. For example, if we rotate the LGM $\Psi_{J; -J+k}(q_\rho, q_\phi)$, which has a constellation with k stars in the south pole and $2J - k$ stars in the north pole, the resulting field will have an equivalent

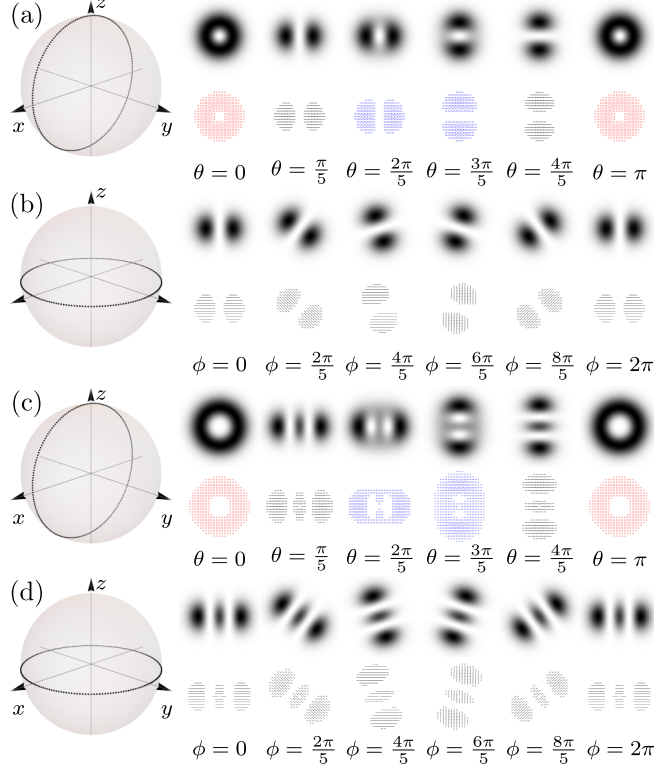


FIG. 7. (Color online) Majorana constellations for the vector light fields analog of Bloch coherent states (a) and (c) $\Psi_{\vartheta,0}(q_\rho, q_\phi)$ and (b) and (d) $\Psi_{\pi/4,\varphi}(q_\rho, q_\phi)$ for (a)-(b) $j = 1$ and (c)-(d) $j = 3/2$. Each set depicts the Majorana constellation (left), intensity (top), and polarization distribution (bottom) for the vector light field. Red, blue and black indicate left-handed, right-handed, and linear polarization, respectively.

antipodal distribution.

B. Cat codes and Kings of Quantumness

As in the scalar case, vector cat codes,

$$\langle q_\rho, q_\phi | C_{\vartheta,\varphi}^0 \rangle = \frac{1}{\sqrt{\cos^{4j} \vartheta + \sin^{4j} \vartheta}} \left[\cos^{2j} \vartheta \Psi_{J,J}(q_\rho, q_\phi) + (e^{i\varphi} \sin \vartheta)^{2j} \Psi_{J,-J}(q_\rho, q_\phi) \right], \quad (28)$$

$$\langle q_\rho, q_\phi | C_{\vartheta,\varphi}^m \rangle = e^{im\varphi} \Psi_{J;J-m}(q_\rho, q_\phi),$$

yield the vector light fields analogues of TAM Dicke states, with the exception of the zeroth cat code, which provides a superposition of the first and last TAM Dicke states in the basis. Figure 8 shows the four vector field cat codes for Bargmann parameter $J = 2$. The first row shows the Majorana constellation on the Riemann sphere. The second row shows the

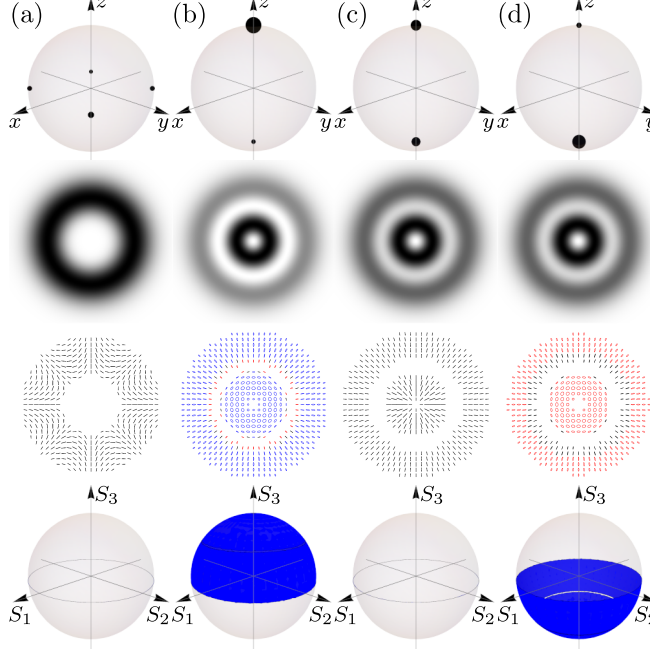


FIG. 8. (Color online) Majorana constellations for vector light fields analogues to (a) zeroth through (d) third cat codes with $\vartheta = \pi/4$ and $\varphi = 0$ for $J = 2$. Each set depicts the Majorana constellation (first row), intensity (second row) and polarization (third row) distributions, and Poincaré sphere (fourth row) for the vector light field. Red, blue and black indicate left-handed, right-handed, and linear polarization, respectively.

irradiance distribution provided by the zeroth component of the stokes parameters S_0 . The third row shows the polarization distribution in the plane transverse to propagation. The fourth row shows the polarization states in the Poincaré sphere. None of the vector light fields cat codes have well defined polarization. The zeroth, Fig. 8(a), and second, Fig. 8(c), are partial Poincaré fields showing all possible linear polarizations. The first, Fig. 8(b), and fourth, Fig. 8(d), show partial Poincaré fields showing all possible left- and right-handed polarizations, in that order. For visualization and clarity purposes, Fig. 9 presents the polarization distribution for the vector light fields analogues of the zeroth to third cat codes with parameters $\vartheta = \pi/4$, $\varphi = 0$ for $J = 2$, with scaling adjusted for illustrative purposes.

It is also possible to produce vector light fields from a Majorana constellation using the procedure outlined in the previous section. The solution to the scalar inverse problem provides the coefficients $C_{J,M}$ for the light field, Eq. 24, corresponding to the Majorana constellation. Then, we substitute the total angular momentum light field, Eq. 25, to

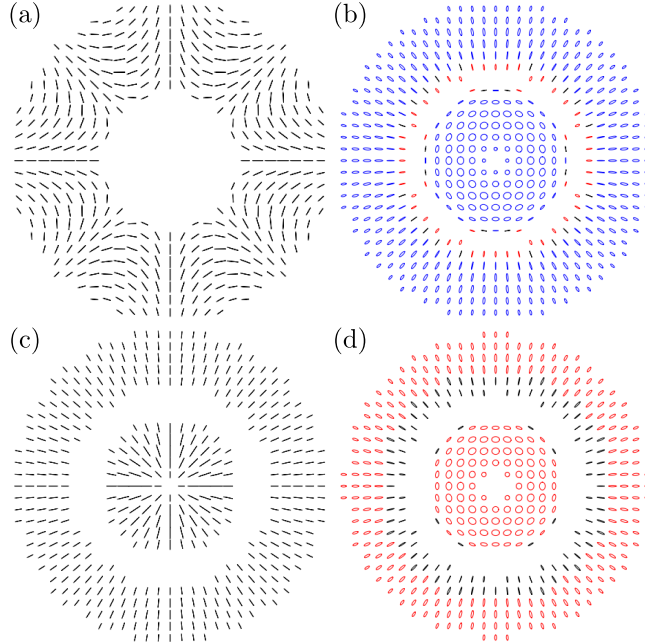


FIG. 9. (Color online) Polarization distribution for vector light fields analogues to (a) zeroth through (d) third cat codes with parameters $\vartheta = \pi/4$, $\varphi = 0$ for $J = 2$. Red, blue and black indicates left-handed, right-handed, and linear polarization, respectively.

recover the polarization and spatial modes components of the light field. For example, starting from the Majorana constellation composed by the vertices of a Platonic solid in the Riemann sphere, we generate the corresponding vector light field [40], Fig. 10. These states are the optical field analogues of the kings of quantumness and do not show a well defined polarization. Those whose Majorana constellation possess reflection symmetry with respect to the three axis in the Riemann sphere show all possible linear polarization, Fig. 10(b) and Fig. 10(c). Those without the symmetry cover most of the Poincaré sphere with two missing polarization regions keeping them from becoming full Poincaré fields. For clarity in visualization, Fig. 11 shows the polarization of vector light fields with star constellations located at the vertices of four platonic solids, with scaling adjusted for illustrative purposes.

IV. CONCLUSION

We used Majorana stellar representation for angular momentum states to construct and visualize optical scalar beams and vector fields as Majorana constellations on the Riemann sphere. This approach leverages the analogy between the polarization and spatial degrees of

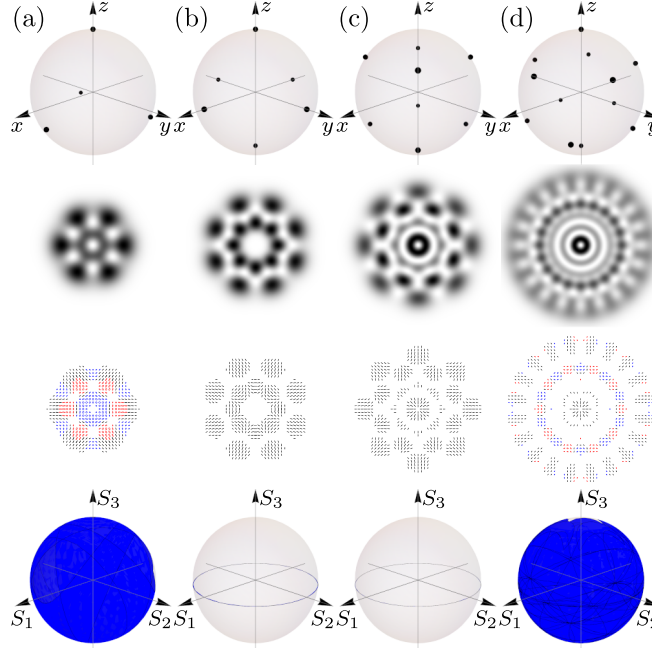


FIG. 10. (Color online) Majorana constellations for vector light fields with stars located at the vertices of four platonic solids, (a) tetrahedron $j = 2$, (b) octahedron $j = 3$, (c) hexahedron $j = 4$, and (d) dodecahedron $j = 6$. Each set depicts the Majorana constellation (first row), intensity (second row) and polarization (third row) distributions, and Poincaré sphere (fourth row) for the vector light field. Red, blue and black indicate left-handed, right-handed, and linear polarization, respectively.

freedom of light with spin and orbital angular momenta, providing a systematic framework to visualize higher-order orbital angular momentum scalar beams and total angular momentum vector fields.

Scalar Laguerre-Gaussian beams provide orthogonal bases for subspaces with constant orbital angular momentum, mapping onto constellations residing at the poles of the Riemann sphere. Constellations for scalar Hermite-Gaussian beams, on the other hand, reside at the equator. Constellations on the sphere are generated through generalized unitary rotations, and their coherent superpositions, provided by the $su(2)$ Lie algebra structure of these subspaces. Interestingly, scalar optical analogues of cat codes, quantum states robust to dephasing, reduce to Laguerre-Gaussian beams. On the other hand, analogues to kings of quantumness, used to align reference frames in quantum communications, exhibit irradiance and phase distributions that allow identifying rotations in the plane transverse to

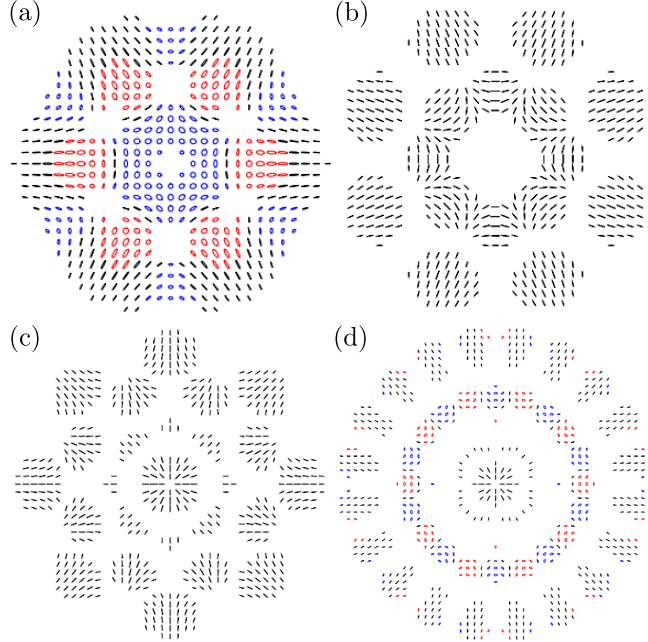


FIG. 11. Polarization distribution for vector light fields with stars located at the vertices of four platonic solids, (a) tetrahedron $j = 2$, (b) octahedron $j = 3$, (c) hexahedron $j = 4$, and (d) dodecahedron $j = 6$. Red, blue and black indicates left-handed, right-handed, and linear polarization, respectively.

propagation.

Including the circular polarization basis yields orthogonal bases for subspaces with constant total angular momentum. Constellations residing at the poles of the Riemann sphere correspond to vector fields with well-defined circularly polarized light, while those on the equator correspond to partial Poincaré fields showing all possible linear polarization states. Constellations on the sphere are generated through generalized unitary rotations and their coherent superpositions. Vector field analogues of cat codes are partial Poincaré fields restricted to linear, left-, or right-handed polarization states. Analogues to kings of quantumness show irradiance distributions that allow identifying rotations. Additionally, those with constellations symmetric with respect to the coordinate axes are partial Poincaré fields showing all linear polarization states, while those without such a symmetry display almost all possible polarization states.

Experimental construction of the optical scalar beams and vector fields represented by our theory can be achieved through established techniques in optics. Scalar beams require

complex amplitude modulation, which can be implemented using phase-only Spatial Light Modulators (SLMs) or Digital Micromirror Devices (DMDs). Computer-generated holography, a widely available method in optics laboratories, provides an effective means for this purpose [46–48]. Vector fields require precise control over both the transverse complex amplitude and electromagnetic field orientation. A standard approach involves preparing each orthogonal component of the electromagnetic field separately and then combining them through an interferometric setup [49]. Recent advancements have introduced additional methods for this process [50–53]. Finally, spatially varying polarization states across the transverse plane can be measured using conventional Stokes polarimetry [54, 55].

We believe Majorana stellar representation offers a powerful framework to visualize, analyze, and propose complex optical beams and fields with higher-order angular momentum, creating a bridge between optical physics and quantum optics to enhance our understanding and control in the tailoring of light.

FUNDING

Not applicable.

ACKNOWLEDGMENT

B. M. R. L. is grateful to Miguel Ángel Avendaño Bernal for fruitful discussion.

DISCLOSURES

The authors declare no conflicts of interest.

DATA AVAILABILITY

Data underlying the results presented in this paper may be obtained from the authors upon reasonable request.

- [1] M. Born and E. Wolf, *Principles of optics*, seventh ed. (Cambridge University Press, Cambridge, 2019).
- [2] Y. B. Konstantin and F. Nori, Transverse and longitudinal angular momenta of light, *Phys. Rep.* **592**, 1 (2015).
- [3] R. C. Jones, A new calculus for the treatment of optical systems I. Description and discussion of the calculus, *J. Opt. Soc. Am.* **31**, 488 (1941).
- [4] U. Fano, A Stokes-parameter technique for the treatment of polarization in quantum mechanics, *Phys. Rev.* **93**, 121 (1954).
- [5] A. Z. Goldberg, P. de la Hoz, G. Björk, A. B. Klimov, M. Grassl, G. Leuchs, and L. L. Sánchez-Soto, Quantum concepts in optical polarization, *Adv. Opt. Photon.* **13**, 1 (2021).
- [6] A. T. O’Neil, I. MacVicar, L. Allen, and M. J. Padgett, Intrinsic and extrinsic nature of the orbital angular momentum of a light beam, *Phys. Rev. Lett.* **88**, 053601 (2002).
- [7] A. E. Siegman, Wave optics and Gaussian beams, in *Lasers* (University Science Books, Mill Valley, Calif, 1986) Chap. 16.
- [8] W. N. Plick and M. Krenn, Physical meaning of the radial index of Laguerre-Gauss beams, *Phys. Rev. A* **92**, 063841 (2015).
- [9] L. Allen, M. W. Beijersbergen, R. J. C. Spreeuw, and J. P. Woerdman, Orbital angular momentum of light and the transformation of Laguerre-Gaussian laser modes, *Phys. Rev. A* **45**, 8185 (1992).
- [10] F. T. Arecchi, E. Courtens, R. Gilmore, and H. Thomas, Atomic coherent states in quantum optics, *Phys. Rev. A* **6**, 2211 (1972).
- [11] E. Majorana, Atomi orientati in campo magnetico variabile, *Nuovo Cim.* **9**, 43 (1932).
- [12] F. Bloch and I. I. Rabi, Atoms in variable magnetic fields, *Rev. Mod. Phys.* **17**, 237 (1945).
- [13] I. Bengtsson and K. Życzkowski, *Geometry of quantum states: an introduction to quantum entanglement*, 1st ed. (Cambridge University Press, 2006).

- [14] G. Björk, A. B. Klimov, P. de la Hoz, M. Grassl, G. Leuchs, and L. L. Sánchez-Soto, Extremal quantum states and their Majorana constellations, *Phys. Rev. A* **92**, 031801 (2015).
- [15] G. Björk, M. Grassl, P. de la Hoz, G. Leuchs, and L. L. Sánchez-Soto, Stars of the quantum universe: extremal constellations on the Poincaré sphere, *Phys. Scr.* **90**, 108008 (2015).
- [16] R. Gutiérrez-Cuevas, S. A. Wadood, A. N. Vamivakas, and M. A. Alonso, Modal Majorana sphere and hidden symmetries of structured-Gaussian beams, *Phys. Rev. Lett.* **125**, 123903 (2020).
- [17] C.-F. Kam and R.-B. Liu, Berry phases of higher spins due to internal geometry of Majorana constellation and relation to quantum entanglement, *New J. Phys.* **23**, 073020 (2021).
- [18] J. Zimba, “Anticoherent” spin states via the Majorana representation, *Electron. J. Theor. Phys.* , 143 (2006).
- [19] J. L. Romero, A. B. Klimov, A. Z. Goldberg, G. Leuchs, and L. L. Sánchez-Soto, Multipoles from Majorana constellations, *Phys. Rev. A* **109**, 012214 (2024).
- [20] P. Kolenderski and R. Demkowicz-Dobrzanski, Optimal state for keeping reference frames aligned and the platonic solids, *Phys. Rev. A* **78**, 052333 (2008).
- [21] F. Bouchard, P. de la Hoz, G. Björk, R. W. Boyd, M. Grassl, Z. Hradil, E. Karimi, A. B. Klimov, G. Leuchs, J. Řeháček, and L. L. Sánchez-Soto, Quantum metrology at the limit with extremal Majorana constellations, *Optica* **4**, 1429 (2017).
- [22] A. Baecklund and I. Bengtsson, Four remarks on spin coherent states, *Phys. Scr.* **2014**, 014012 (2014).
- [23] C. He, Y. Shen, and A. Forbes, Towards higher-dimensional structured light, *Light Sci. Appl.* **11**, 205 (2022).
- [24] M. J. Padgett and J. Courtial, Poincaré-sphere equivalent for light beams containing orbital angular momentum, *Opt. Lett.* **24**, 430 (1999).
- [25] G. F. Calvo, Wigner representation and geometric transformations of optical orbital angular momentum spatial modes, *Opt. Lett.* **30**, 1207 (2005).
- [26] S. J. M. Habraken and G. Nienhuis, Universal description of gemometric phases in higher-order optical modes bearing orbital angular momentum, *Opt. Lett.* **35**, 3535 (2010).
- [27] G. Milione, H. I. Sztul, D. A. Nolan, and R. R. Alfano, Higher-order Poincaré sphere, Stokes parameters, and the angular momentum of light, *Phys. Rev. Lett.* **107**, 053601 (2011).

- [28] X. Yi, Y. Liu, X. Ling, X. Zhou, Y. Ke, H. Luo, S. Wen, and D. Fan, Hybrid-order Poincaré sphere, *Phys. Rev. A* **91**, 023801 (2015).
- [29] Y. Shen, Z. Wang, X. Fu, D. Naidoo, and A. Forbes, $Su(2)$ Poincaré sphere: A generalized representation for multidimensional structured light, *Phys. Rev. A* **102**, 031501(R) (2020).
- [30] M. P. Morales Rodríguez, O. S. Magaña-Loaiza, B. Perez-Garcia, L. M. Nieto Calzada, F. Marroquín Gutiérrez, and B. M. Rodríguez-Lara, Coherent states of the Laguerre-Gauss modes, *Opt. Lett.* **49**, 1489 (2024).
- [31] M. P. Morales Rodríguez, E. García Herrera, O. S. Magaña-Loaiza, B. Perez-Garcia, F. Marroquín Gutiérrez, and B. M. Rodríguez-Lara, Spatial light mode analogues of generalized quantum coherent states, *Phys. Rev. A* **110**, 033523 (2024), arXiv:2406.00169 [physics.optics].
- [32] J. Schwinger, Harmonic oscillators, in *Quantum mechanics: symbolism of atomic measurements* (Springer, Berlin, Heidelberg, 2001) pp. 269–302.
- [33] L. Villanueva Vergara and B. M. Rodríguez-Lara, Gilmore-Perelomov symmetry based approach to photonic lattices, *Opt. Express* **23**, 22836 (2015).
- [34] E. Abramochkin and V. G. Volostnikov, Generalized Gaussian beams, *J. Opt. A: Pure Appl. Opt.* **6**, S157 (2004).
- [35] L. Li, C.-L. Zou, V. V. Albert, S. Muralidharan, S. M. Girvin, and L. Jiang, Cat codes with optimal decoherence suppression for a lossy bosonic channel, *Phys. Rev. Lett.* **119**, 030502 (2017).
- [36] Z. Leghtas, G. Kirchmair, B. Vlastakis, R. J. Schoelkopf, M. H. Devoret, and M. Mirrahimi, Hardware-efficient autonomous quantum memory protection, *Phys. Rev. Lett.* **111**, 120501 (2013).
- [37] M. Mirrahimi, Z. Leghtas, V. V. Albert, S. Touzard, R. J. Schoelkopf, L. Jiang, and M. H. Devoret, Dynamically protected cat-qubits: a new paradigm for universal quantum computation, *New J. Phys.* **16**, 045014 (2014).
- [38] A. L. Grimsmo, J. Combes, and B. Q. Baragiola, Quantum computing with rotation-symmetric bosonic codes, *Phys. Rev. X* **10**, 011058 (2020).
- [39] H. Gray Funkhouser, A short account of the history of symmetric functions of roots of equations, *Am. Math. Mon.* **37**, 357 (1930).
- [40] R. Gutiérrez-Cuevas and M. Alonso, Platonic Gaussian beams: wave and ray treatment, *Opt. Lett.* **45**, 6759 (2020).

- [41] A. Alex, M. Kalus, A. Huckleberry, and J. von Delft, A numerical algorithm for the explicit calculation of $SU(N)$ and $SL(N, C)$ Clebsch–Gordan coefficients (2011), arXiv:1009.0437.
- [42] D. J. Griffiths and D. F. Schroeter, *Introduction to Quantum Mechanics* (Cambridge University Press, Cambridge, UK, 2019).
- [43] M. A. Alonso and M. R. Dennis, Ray-optical Poincaré sphere for structured Gaussian beams, *Optica* **4**, 476 (2017).
- [44] A. M. Perelomov, Coherent states for arbitrary Lie group, *Commun. Math. Phys.* **26**, 222 (1972).
- [45] W.-M. Zhang, D. H. Feng, and R. Gilmore, Coherent states: theory and some applications, *Rev. Mod. Phys.* **62**, 867 (1990).
- [46] V. Arrizón, U. Ruiz, R. Carrada, and L. A. González, Pixelated phase computer holograms for the accurate encoding of scalar complex fields, *J. Opt. Soc. Am. A* **24**, 3500 (2007).
- [47] A. Forbes, A. Dudley, and M. McLaren, Creation and detection of optical modes with spatial light modulators, *Adv. Opt. Photon.* **8**, 200 (2016).
- [48] R. Gutiérrez-Cuevas and S. M. Popoff, Binary amplitude holograms for shaping complex light fields with digital micromirror devices, *J. Phys. Photonics* **6**, 045022 (2024).
- [49] S. C. Tidwell, D. H. Ford, and W. D. Kimura, Generating radially polarized beams interferometrically, *Appl. Opt.* **29**, 2234 (1990).
- [50] C. Maurer, A. Jesacher, S. Fürhapter, S. Bernet, and M. Ritsch-Marte, Tailoring of arbitrary optical vector beams, *New J. Phys.* **9**, 78 (2007).
- [51] Z. Chen, T. Zeng, B. Qian, and J. Ding, Complete shaping of optical vector beams, *Opt. Express* **23**, 17701 (2015).
- [52] I. Moreno, J. A. Davis, M. M. Sánchez-López, K. Badham, and D. M. Cottrell, Nondiffracting Bessel beams with polarization state that varies with propagation distance, *Opt. Lett.* **40**, 5451 (2015).
- [53] C. Rosales-Guzmán, X.-B. Hu, A. Selyem, P. Moreno-Acosta, S. Franke-Arnold, R. Ramos-Garcia, and A. Forbes, Polarisation-insensitive generation of complex vector modes from a digital micromirror device, *Sci. Rep.* **10**, 10434 (2020).
- [54] D. Goldstein, *Polarized light* (CRC Press, 2017).
- [55] K. Singh, N. Tabebordbar, A. Forbes, and A. Dudley, Digital Stokes polarimetry and its application to structured light: tutorial, *J. Opt. Soc. Am. A* **37**, C33 (2020).